

## Nondestructive DC Beam Current Monitor with NANO-Ampere Resolution

Yuuichirou SASAKI, Kichiji HATANAKA, Kenji SATO, Tetsumi TANABE\*,  
Shinpei ONO\*, Kouji NODA\*\*, Kei SHINADA\*\*\*, Yasuharu YAMADA\*\*\* and Kouichi NAKANO\*\*\*  
Research Center for Nuclear Physics, Osaka Univ.,  
Osaka 567 JAPAN

\*Center for Nuclear Study, School of Science, Univ. of Tokyo,  
Tokyo 188 JAPAN

\*\*National Institute of Radiological Sciences,  
Chiba 263 JAPAN

\*\*\*Technology Research Laboratory, Shimadzu Corporation,  
Kyoto 619-02 JAPAN

### Abstract

A beam intensity monitor using a SQUID is being designed in order to measure the ion beam intensity in a non-destructive manner. Prior to the design procedure, some fundamental tests were performed with models. Measurements were performed to investigate sensitivities, shielding effects, and noise levels of the system. Results are described, and the design of a cryostat is also presented.

### 1 Introduction

There are various detection systems developed to measure beam intensities from accelerators. Scintillators cover the region up to  $10^6$  particles per second (pps), corresponding to electrical currents up to 1 pA. Current transformers of the fluxgate type can cover the region over some  $\mu\text{A}$  in a non-destructive manner. The region in between can be covered by ionization chambers (IC) and secondary emission monitors (SEM). But these systems more or less distort the ion beam due to the energy loss and the beam emittance growth by scatterings. Another type of beam transformer, using the principle of a Cryogenic Current Comparator<sup>1</sup> (CCC), is being designed at the Research Center for Nuclear Physics (RCNP), Osaka University in collaboration with the National Institute of Radiological Sciences (NIRS). In the design, a DC-SQUID is adopted to improve the resolution. The nA resolution is expected.

### 2 A SQUID System

Figure 1 shows the circuit diagram of a SQUID and a flux locked loop. SQUID, the pick up, the input and the feedback coils are coupled.

$$(L_p + L_i)I_p + M_{fi}I_f = \Phi_p$$

$$M_{is}I_p + M_{fs}I_f = \Phi_x$$

where  $L_p$  is the pick up coil inductance,  $L_i$  the input coil inductance (200 nH),  $M_{fi}$  is the mutual inductance between the input coil and the feedback coil (6 nH),  $M_{is}$  between the input coil and SQUID (5 nH),  $M_{fs}$  between the feedback coil and SQUID (2.2 pH),  $I_p$  is the current through the input coil,  $I_f$  through the feedback coil and  $\Phi_p$  is the flux which penetrates the pick up coil,  $\Phi_x$  penetrates the SQUID washer.

If a dc bias current is fed to SQUID, the voltage  $V_s$  changes periodically depending on  $\Phi_x$  with  $\Phi_0$  period. Where  $\Phi_0$  is the flux quantum;  $\Phi_0 = 2.07 \times 10^{-15}$  Wb.  $\Phi_p$  is proportional to the beam current  $I_b$ . The current  $I_f$  is fixed under the condition  $I_b = 0$ , and the flux  $\Phi_x$  is locked. When  $I_b$  is fed, the feedback current  $I_f$  flows to keep the flux  $\Phi_x$  constant. This change in  $I_f$  is proportional to the current  $I_b$ .

In the present design, a double washer DC SQUID developed as a magnetic-flux sensor for a multichannel biomagnetometer at Shimadzu Corporation<sup>2</sup> was used as the magnetic flux sensor. The measuring principle is the same as described above.

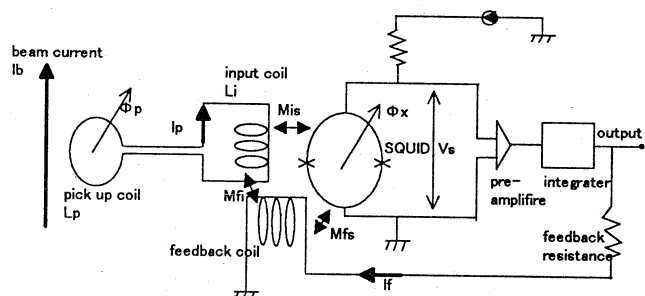


Fig. 1 Circuit diagram of a SQUID and flux locked loop.

### 3 Test with Small Size Models

Models were fabricated to examine the performance of the system. Figure 2 shows one of them. The system consists of a magnetic shielding, a pick up coil, and a SQUID circuit. The beam current is simulated with a one turn loop around the magnetic shielding. The loop current induces an azimuthal magnetic field. Because of the shielding structure, the azimuthal component of the magnetic field can penetrate into the shielding with small attenuation, while other components are strongly attenuated. In order to realize high sensitivity, it is necessary to reduce noises around the pick up

coil and the SQUID. Measurements were performed to investigate sensitivities, noise structures, and shielding effects of the system using a FINEMET (Hitachi Metals, FT-3L, FT-3M) or an amorphous (VITROVAC 6025-F) toroidal core surrounded by 4 turns of NbTi wire.

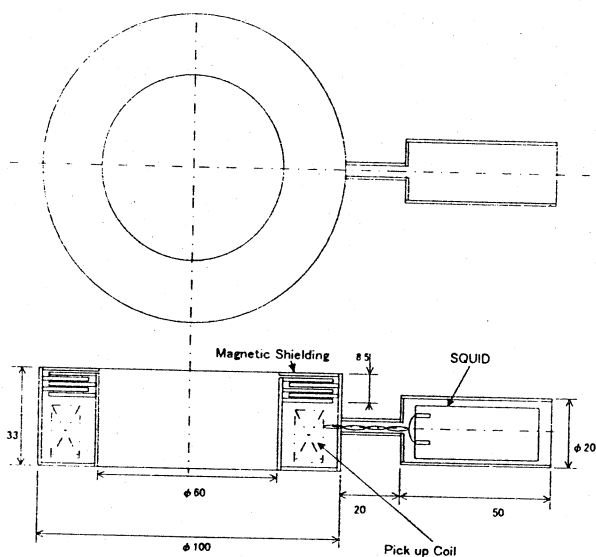


Fig. 2 Schematic drawings of the model. The magnetic shielding is a folder type with five ring type shield elements. A FINEMET or an amorphous toroidal core surrounded by 4 turns of NbTi wire is used as the pick up coil.

### 3.1 Sensitivity

Responses were measured with 600 nA, dc current. Sensitivities are independent of the number of shielding elements, but they depend on the kind of a toroidal core. Table 1 shows obtained sensitivities. These values are consistent with those expected from the calculation. When a FINEMET or an amorphous toroidal core was used, sensitivities were about 1 mV/nA·kΩ. With an air core, sensitivity was lower (1/500 of magnitude) than those with a VITROVAC 6025-F or a FT-3L toroidal core.

Table 1  
Sensitivities obtained with models.

Kind of a toroidal core	Sensitivity	Feedback resistance
VITROVAC 6025-F	3 mV/nA	4.7 kΩ
FT-3L	0.92 mV/nA	1 kΩ
FT-3M	8.3 mV/nA	4.7 kΩ
air	0.14 mV/nA	100 kΩ

### 3.2 Noise

The origins of noises are supposed to be electromagnetic noises, mechanical movements of the system, and from the characteristics of toroidal cores. The frequency of main electromagnetic noise is 60 Hz. Mechanical movements of the system give 1-30 Hz noises. Table 2 shows the measured noise levels using four kinds of a toroidal core. The noise level with a FT-3M core is 2 orders of magnitude larger than those with a VITROVAC 6025-F or a FT-3L core. This may come from the fact that the remanent magnetic flux density of FT-3M is higher than those of VITROVAC 6025-F and FT-3L.

Table 2  
The measured noise levels using four kinds of a toroidal core. The low pass filter was not installed.

Kind of a toroidal core	Noise level	Feedback resistance
VITROVAC 6025-F	40 mV	4.7 kΩ
FT-3L	15 mV	1 kΩ
FT-3M	1500 mV	4.7 kΩ
air	18 mV	100 kΩ

Noise spectra were measured. It was found that each core has noises of characteristic frequencies. Noises at 15, 30, 32, 33, 40, 72, and 80 Hz appeared in case of a FT-3L toroidal core (see Figure 3). In case of a VITROVAC 6025-F toroidal core, a noise at 32 Hz appeared, and in a FT-3M toroidal core at 33 and 90 Hz.

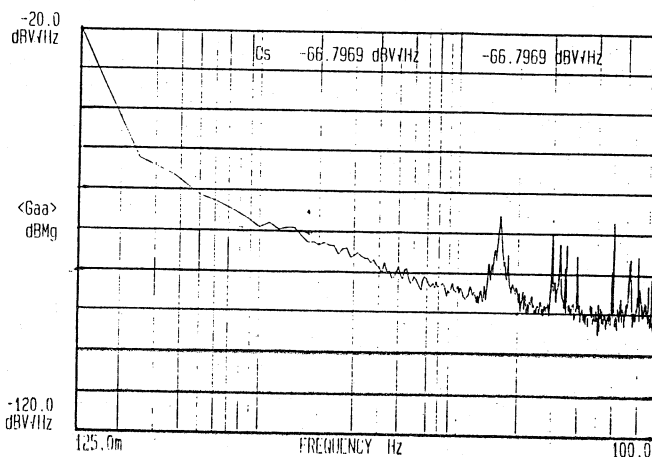


Fig. 3 The noise spectrum measured with a FT-3L toroidal core. The low pass filter was not installed.

A low pass filter whose cut-off frequency was 10 Hz was installed in the system. When the low pass filter was used, the noise levels were become 1/3 of magnitude smaller than those values in Table 2. Main effect is that 60 Hz electromagnetic noise was reduced to 1/3 of magnitude. The measured sensitivities were the same as those in Table 1. Figure 4 shows a series of 10 nA test pulses with the low pass filter. The signal indicates a movement of the base line in the order of 0.5 nA/s.

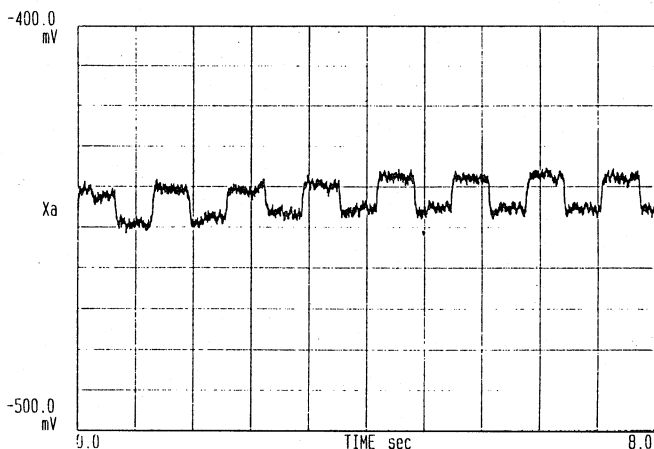


Fig. 4 10 nA pulses, 0.5 s pulse width with a low pass filter. A FT-3L toroidal core is used. (horizontal axis: 0.8 sec/div., vertical axis: 10 mV/div.)

### 3.3 Shielding Efficiency

The shielding efficiency was studied for three cavities with a VITROVAC 6025-F toroidal core. They are the cavities which have one ring type shielding element, five ring type elements and two coaxial type elements, respectively. Each cavity has been exposed to uniform external magnetic fields with Helmholtz coils wound outside of the cryostat. An external field of  $10^{-5}$  T gave signals corresponding to 10-700 nA (see Table 3). When the cavity which has five ring type shielding elements was exposed to a transverse external field of  $10^{-5}$  T, the signal corresponding to 30 nA was yielded. This value is lower by 1/5 times than expected from the calculation, but it is still higher by an order of magnitude than that required for the environment in which this system will be installed. When the cavity which has two coaxial type elements was exposed to a transverse external field of  $10^{-5}$  T, the change of signal could not be observed. The theoretical prediction is  $5 \times 10^{-4}$  nA. This small change cannot be resolved in our experiment because of the limits of measurement.

### 4 The cryostat

A schematic drawing of the cryostat is shown in Figure 6. A warm hole of 110 mm in diameter is required in order to pass the beam. Isolation gaps using  $Al_2O_3$

Table 3  
The shielding efficiency.

Shielding elements	$\vec{B} \parallel \vec{I}$	$\vec{B} \perp \vec{I}$
1 ring	20 nA	730 nA
5 ring	9 nA	30 nA
2 coaxial	less than $8 \times 10^{-3}$ nA	less than $2 \times 10^{-2}$ nA

ceramics are inserted into both the beam tube and the liquid He container tube to avoid effects from wall currents. Side walls of the cryostat can be dismantled to exchange a shield and a SQUID system. Three layers of heat radiation shields, two super insulations and a copper shield, are equipped to minimize the heat conduction. Stock volume of liquid He is 15 l. The cryostat is now under construction.

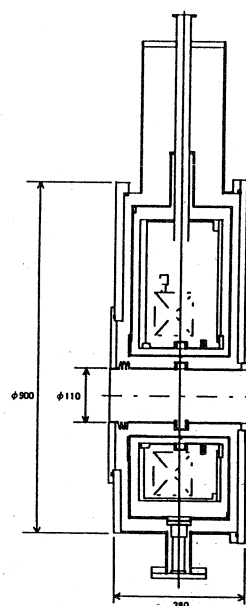


Fig. 5 Cryostat under construction.

### References

- [1] A. Peters et al., "A Cryogenic Current Comparator for Nondestructive Beam Intensity Measurements", Proc. 1994 the Fourth European Part. Accel. Conf., London, (1994) 290.
- [2] K. Shinada et al., Shimadzu Review 51 (1994) 217.